Influence of illumination spectrum on dissociation kinetic of iron-boron pairs in silicon

Oleg Olikh Oleksandr Datsenko Serhiy Kondratenko*

Prof. O. Olikh, Dr. O. Datsenko, Prof. S. Kondratenko
Taras Shevchenko National University of Kyiv, 64/13, Volodymyrska Street, 01601, Kyiv, Ukraine
Email Address: olegolikh@knu.ua

Keywords: *silicon, iron-boron pairs, light-induced dissociation, light source impact*

Please insert your abstract here

1 Introduction

Defects significantly impact semiconductor properties. Although minimizing device dimensions to nanometers shifts some focus from extensive to point defects, physical properties still rely heavily on the presence and distribution of these irregularities. Hence, many strategies for enhancing semiconductor structures, including radiation and temperature treatments or certain fabrication conditions, strive to decrease the defect concentration or neutralize its effects [1, 2, 3]. For instance, in the case of photovoltaic devices, we must understand and optimize the carrier properties tied to defects and impurities [1]. Such controlled alteration methods of the defective subsystem have been generalized under the term "defect engineering" and are extremely important from a practical standpoint.
Successful defect engineering hinges on an in-depth understanding of defect properties. Key factors are defect formation energy, transition energy levels, self-compensating effects, nonradiative recombination caused by defects, and the mechanism of reconstruction and diffusion [1]. Considering the extraordinary diversity of possible intrinsic and impurity defects, complete information on all of them is lacking even for silicon, which is the most studied semiconductor. Nevertheless, it must be noted that considerable data have been amassed on silicon, and have a solid understanding of some defects [4].
For instance, such defects are iron impurity, a common, detrimental, and often unavoidable contaminant in photovoltaic silicon [3, 5], and iron-boron pair. Specifically, iron atoms are known to be at the interstitial sites, and Fe_i^+ are highly efficient recombination centers [6]. In p-type Si at room temperature, iron atoms are almost predominantly bound in complexes with dopants (B, Ga, Al, In). This defect demonstrates bistable behavior: the stable state is defined by the configuration in which the Fe occupies the first nearest tetrahedral interstitial site closest to the substituent atom, whereas, in the metastable configuration, Fe is at the second T_d interstitial site [7]. The energy levels associated with iron and its complexes, as well as the respective carriers capture cross-sections, are well-established [4, 8]. Among the acceptor-iron pairs, the complex FeB is the most thoroughly investigated, primarily due to the widespread use of Si:B in the fabrication of various devices, such as solar cells. However, it is worth mentioning that gallium is gaining increasing attention as an acceptor dopant whose incorporation, for instance, can help mitigate the light and elevated temperature-induced degradation [9].
The dynamics of FeB pairs are also examined. It's established that FeB pairs can be dissociated through illumination, minority carrier injection, and thermal treatment at 200 °C [10]. In the context of illumination, the dissociation rate R_d is influenced by the overall carrier generation rate G [11, 10, 12, 13]:

$$R_d = K\left(\frac{G}{N_{\mathrm{FeB}}}\right)^2, \tag{1}$$

where N_{FeB} is the pair concentration, K is the constant of material. To achieve almost complete dissociation of the FeB pair, it is necessary for the illumination power to exceed 0.1 W cm^{-2} [14]. The dissociation process of FeB pairs by electron capture unfolds in two stages [15, 10]: the initial stage involves

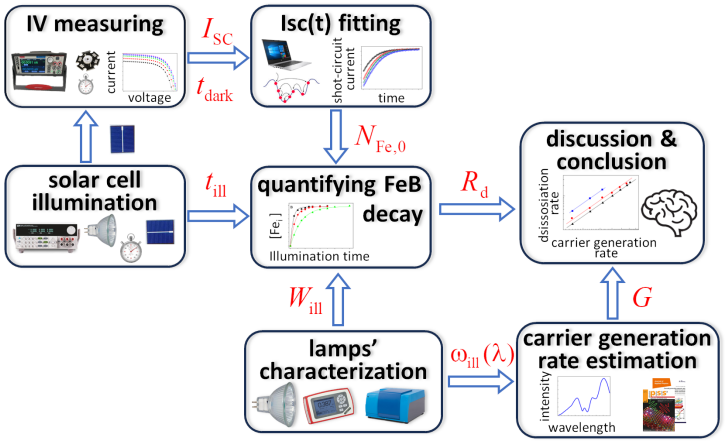

Figure 1: Investigation framework

the neutralization of Fe and the elimination of the Coulombic attraction between the pair components. The mechanism of the second stage is contentious; it may involve either the recharge of the iron ion or the recombination-enhanced defect reaction (REDR) triggered by electron-hole recombination.

It should be noted that despite the extensive data on the properties of iron-related defects in silicon, intensive research persists. In particular, efforts focus on analyzing the impact of high-intensive illumination [16] or dopant compensation [17], alongside clarifying the second-stage mechanism of dissociation [5] or reassessing recombination parameters [18].

This study aims to investigate the effect of the light spectrum on the dissociation kinetics of FeB pairs in silicon. While pair dissociation is typically carried out using a halogen lamp [11, 5] or 904 nm laser [16, 10, 19], there is limited understanding of how the light source influences this process. By studying the impact of different illumination spectra on FeB dissociation, we aim to provide valuable insights for defect engineering and the efficient transformation of detrimental impurity iron atoms into a highly mobile interstitial state within the active region of a silicon device. Besides, such information, in our opinion, can help make the right choice between existing options for the second stage of pair decay.

Figure 1 illustrates the main stages of the research. Initially, the dissociation rate of FeB pairs under illumination of the solar cell with different integrated intensities was determined. For this purpose, the dependence of the quantity of interstitial iron atoms formed over time under intense illumination was measured. The concentrations of formed pairs were measured by investigating the kinetics of short-circuit current. Three light sources from different manufacturers were used (further details are described in Section 1). To determine the carrier generation rate, spectra of sample illumination using various light sources were measured, taking into account the effects of light reflection, absorption by free carriers, and effective absorption depths. The obtained results led to the conclusion that the efficiency of light-induced dissociation increases with decreasing photon wavelength.

In Figure 1, the main stages of the research are illustrated. First step was determination of the dissociation rate of FeB pairs under illumination with different integrated intensities. Three light sources from different manufacturers were used (further details are described in Section 4). To measure number of interstitial iron atoms formed over fixed time under strong illumination the kinetics of short-circuit current was used. The result is presented in Section 2.1. Section 2.2 deals with estimating the carrier generation rate using spectra of sample illumination and considering the effects of light reflection, absorption by free carriers, and effective absorption depths. The obtained results showed that the efficiency of light-induced dissociation increases with decreasing photon wavelength — see Section 2.3. Finally, we conclude this paper in Section 3.

2 Results and Discussion

2.1 Dissociation rate determination

The equilibrium between free Fe_i and Fe_iB_s is known to be determined by the following equations [20, 5, 10]

$$Fe_i + B_s \underset{R_d}{\overset{R_a}{\rightleftharpoons}} FeB\,, \tag{2}$$

where R_a is the association rate. As a result, the concentration of interstitial iron atoms N_{Fe_i} depending on illumination time t_{ill} during light-induced dissociation can be described as follows [11, 12, 21]

$$N_{Fe_i}(t_{ill}) = \left(N_{Fe,eq} - N_{Fe,tot}\frac{R_d}{R_d+R_a}\right)\exp[-(R_d+R_a)t_{ill}] + N_{Fe,tot}\frac{R_d}{R_d+R_a}\,, \tag{3}$$

where $N_{Fe,tot}$ is the total concentration of the impurity iron, $N_{Fe,eq}$ represents the concentration of unpaired interstitial iron atoms in the equilibrium state (in darkness, $N_{Fe,eq} = N_{Fe_i}(t_{ill} = 0)$). It's important to highlight that $N_{Fe,eq}$ is significantly influenced by temperature and the Fermi level location [20]. Specifically, in the case of p-type Si with a hole concentration of 1.36×10^{15} cm^{-3} (which corresponds to the base of the structure under investigation), at a temperature of $T = 300$ K, $N_{Fe,eq}$ constitutes merely about 1% of $N_{Fe,tot}$, rendering it negligible for practical considerations. However, when the temperature rises to 340 K, the proportion of $N_{Fe,eq}$ increases to approximately 14.5%.

After the cessation of illumination, only the process of association occurs, and the time dependence of Fe_i concentration can be expressed as follows [20, 22]:

$$N_{Fe_i}(t_{dark}) = (N_{Fe,0} - N_{Fe,eq}) \times \exp(-R_a t_{dark}) + N_{Fe,eq}\,, \tag{4}$$

where t_{dark} is the time after strong illumination stopping, $N_{Fe,0}$ is the concentration of interstitial iron atoms formed after illumination, $N_{Fe,0} = N_{Fe_i}(t_{dark} = 0) = N_{Fe_i}(t_{ill})$.

The study examined the dependence of $N_{Fe,0}$ in silicon solar cells on illumination time t_{ill} using different illumination intensities W_{ill} (200 − 750 mW) and light sources (three halogen lamps, labeled as Orion, Osram, and GE, and described in detail in Section 4). The experiments were conducted at a temperature of 340 K. The values of $N_{Fe,0}$ were determined using a methodology [23, 21] based on the study of the kinetics of short-circuit current I_{SC} under low-intensity monochromatic illumination. Specifically, after strong illumination with a duration of t_{ill}, the current-voltage characteristic (IV) of the solar cell was measured every 21 seconds over a time t_{dark} interval of approximately 3000 seconds.

Figure 2a shows some typical IV curves. It can be seen that upon cessation of illumination, there exists a gradual augmentation in both the short-circuit current and the open-circuit voltage. This phenomenon is indicative of a decrease in the recombination activity of the defective subsystem, which is a result of the transition of interstitial iron to a bound state with an acceptor. Moreover, at the end of the measurement interval, the minute changes in the IV curves denote that the selected interval of 50 minutes is sufficient to complete the association.

Figure 2b illustrates the dependencies $I_{SC}(t_{dark})$ after illumination with different intensities. As previously shown [21], the magnitude of the change in I_{SC} after the dark recovery period inherently correlates with the concentration of Fe_i formed as a result of light-induced dissociation of FeB pairs. From examining the presented data, it is evident that escalating W_{ill} leads to an augmentation in the dissociation efficiency. Concurrently, the recovery time remains insensitive to the illumination parameters, which conforms to expectations, given that the latter is determined by R_a — see Equation (4).

Reassessing iron–gallium recombination activity in silicon [18]
AIPAdv 3 082124 [16]
Effect of Dopant Compensation on the Behavior of Dissolved Iron and Iron-Boron Related Complexes in Silicon InterJPhotoener 2015 154574 [17]
JApplPhys 116 024503 [10]
PhysStatSolA 216 1900253 [12]

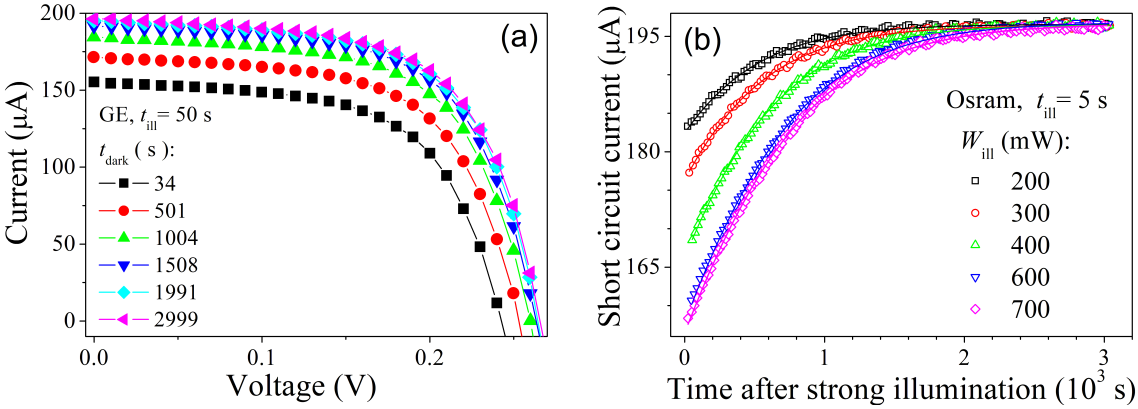

Figure 2: Typical current-voltage characteristics measured under low-intensive (LED) illumination across different periods following exposure to strong light (halogen lamp) (panel a) and short circuit current plotted as a function of the time after high-intensive illumination (panel b). The marks are the experimental results and the lines on panel b are the curves fitted according to [23, 21]. Light sources: GE (a), Osram (b). t_{ill}, s: 50 (a), 5(b). $W_{ill} = 400$ mW (a). $T = 340$ K.

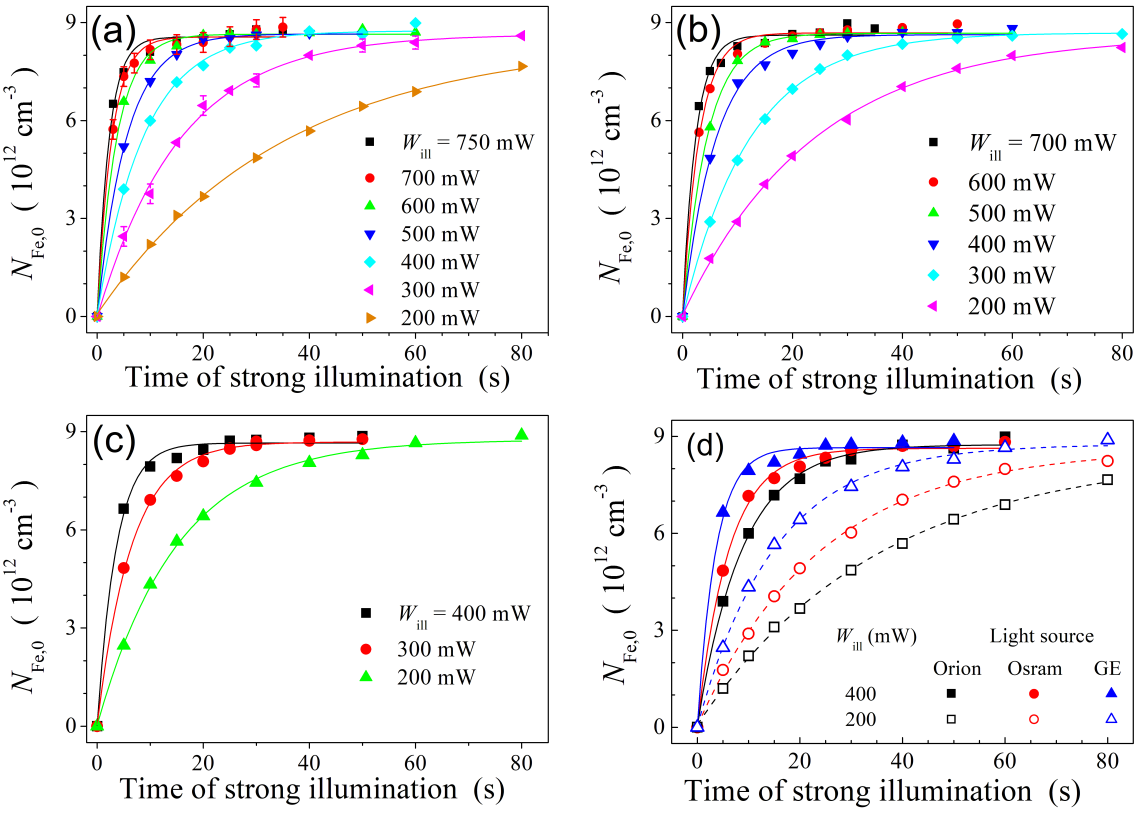

Figure 3: The relationships between the concentration of FeB pairs following intense illuminations of varying intensities and the illumination duration. Light source: Orion (a), Osram (b), GE (c). Panel d highlights variations in the dissociation of pairs induced by different light sources. The marks are the experimental results, the lines are the fitted curves using Equation (**??**). $T = 340$ K.

Table 1: The value of maximum concentrations of iron atoms after illumination and characteristic dissociation time obtained by approximating experimental dependencies by Equation (**??**). Coefficient of determination is listed as well.

W_{ill} [mW]	Light source	τ_{dis} [s]	$N_{Fe,fit}$ [10^{12} cm^2]	R^2
750	Orion	2.2 ± 0.2	8.6 ± 0.1	0.993
700	Orion	2.7 ± 0.2	8.6 ± 0.1	0.995
	Osram	2.4 ± 0.2	8.6 ± 0.1	0.992
600	Orion	3.7 ± 0.2	8.65 ± 0.06	0.998
	Osram	3.0 ± 0.2	8.69 ± 0.08	0.995
500	Orion	5.5 ± 0.2	8.65 ± 0.04	0.999
	Osram	4.5 ± 0.1	8.7 ± 0.1	0.998
400	Orion	8.8 ± 0.3	8.74 ± 0.06	0.998
	Osram	6.1 ± 0.2	8.63 ± 0.08	0.997
	GE	3.6 ± 0.3	8.7 ± 0.1	0.996
300	Orion	15.7 ± 0.6	8.6 ± 0.1	0.998
	Osram	12.4 ± 0.1	8.69 ± 0.02	0.999
	GE	6.5 ± 0.2	8.69 ± 0.05	0.998
200	Orion	35 ± 3	8.5 ± 0.3	0.998
	Osram	24 ± 1	8.6 ± 0.1	0.999
	GE	15.1 ± 0.5	8.7 ± 0.1	0.999

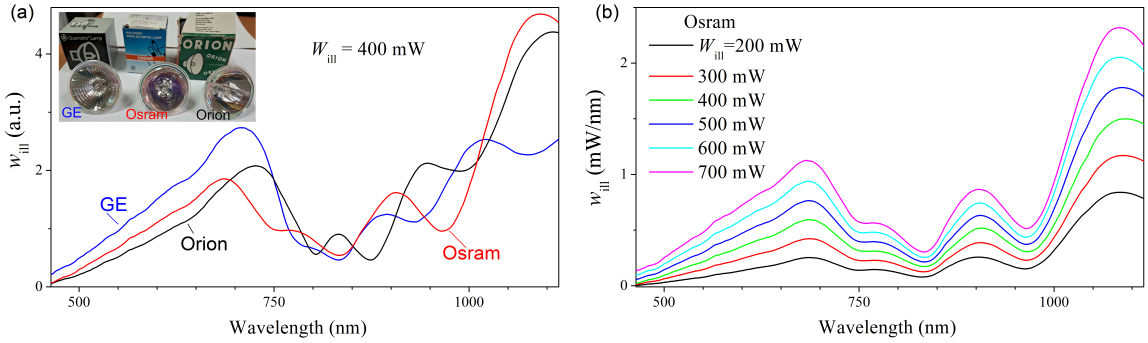

Figure 4: The spectra of sample illumination in the case of using different light sources with the same integrated intensity W_{ill} = 400 mW (panel a) and a single source (Osram) at various W_{ill} values (panel b). The inset shows photos of light sources.

PhysStatSolRRL 15 2100520 [5]
PR ApplPhysLett 85 p5227 5229 [11]
PR JApplPhys 98 083509 [24]
SolStPhenom 242 p230 [19]
JApplPhys 95 p1021 [14]
PR PhysStSolRRL 6 p1 [13]

2.2 Carrier generation rate estimation

A part of the radiation especially in the near infrared region of the spectrum is modified by infrared transparency of the reflector and by absorption in the plexiglass window. [25]
d_{eff} [26]
A_{bb} [27]
α_{bb}, refractive index n [28]
α_{fca} [29]

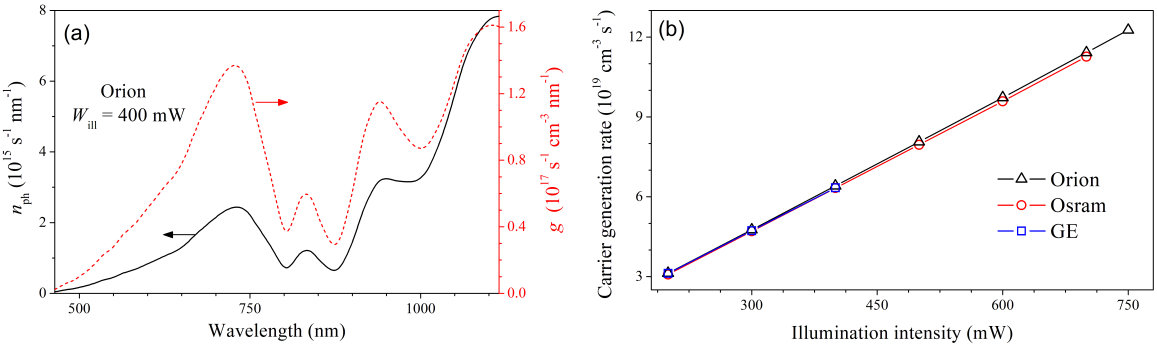

Figure 5: (a) Photon flux spectral density (left axis, solid line) and carrier generate rate spectral density (right axis, dashed line). Orion light source, $W_{\text{ill}} = 400$ mW. (b) Dependencies of carrier generation rate on illumination intensity for different light sources.

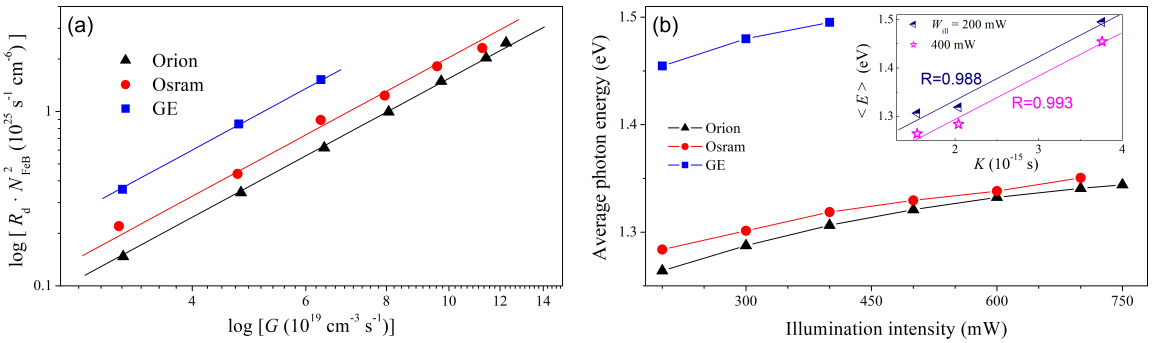

Figure 6: (a) FeB pair dissociation rate plotted as $R_d \cdot N_{\text{FeB}}^2$ over the light induced generation rate. The solid lines show the quadratic dependence according to Equation (1). (b) Dependencies of average photon energy on illumination intensity for different light sources. The inset shows prefactor K vs average photon energy for the different light sources and illumination intensities. The lines are linear fitted curves. Coefficients of correlation are shown as well.

2.3 Effect of illumination spectrum on FeB pair decay

3 Conclusion

[30, 8, 20],[31, 32, 33],
Klyui *et al.*[34])
As explained in Refs.[6,21], the local vibrational energy released from a recombination event at the defect center can promote defect reactions such as dissociation and diffusion.

4 Experimental Section

The temperature was maintained constant using a PID (proportional-integral-derivative controller) algorithm which is implemented in the software which serves the system.
Therefore, the temperature of the wafers was regulated and controlled through a thermoelectric cooling system based on the Peltier effect

First part of experimental section:

Second part of experimental section:

Supporting Information
Supporting Information is available from the Wiley Online Library or from the author.

Acknowledgements
The authors are grateful for the help with calculating the coefficient of reflection by solar cells to Prof. Vitaliy Kostylyov.

Conflict of Interest The authors declare no conflict of interest.

References

[1] X. Cai, S.-H. Wei, *J. Appl. Phys.* **2023**, *134*, 22 220901.

[2] J. Vobecky, *Phys. Status Solidi A* **2021**, *218*, 23 2100169.

[3] J. Frascaroli, P. Monge Roffarello, I. Mica, *Phys. Status Solidi A* **2021**, *218*, 23 2100206.

[4] M. K. Juhl, F. D. Heinz, G. Coletti, D. Macdonald, F. E. Rougieux, F. Schindle, T. Niewelt, M. C. Schubert, In *2018 IEEE 7th World Conference on Photovoltaic Energy Conversion (WCPEC) (A Joint Conference of 45th IEEE PVSC, 28th PVSEC & 34th EU PVSEC)*. **2018** 0328–0332.

[5] C. Sun, Y. Zhu, M. Juhl, W. Yang, F. Rougieux, Z. Hameiri, D. Macdonald, *Phys. Status Solidi RRL* **2021**, *15*, 12 2000520.

[6] E. Weber, *Appl. Phys. A* **1983**, *30*, 1 1.

[7] H. Nakashima, T. Sadoh, T. Tsurushima, *Phys. Rev. B* **1994**, *49*, 24 16983.

[8] F. E. Rougieux, C. Sun, D. Macdonald, *Sol. Energy Mater. Sol. Cells* **2018**, *187* 263 .

[9] L. Ning, L. Song, J. Zhang, *J. Alloys Compd.* **2022**, *912* 165120.

[10] C. Möller, T. Bartel, F. Gibaja, K. Lauer, *J. Appl. Phys.* **2014**, *116*, 2 024503.

[11] L. J. Geerligs, D. Macdonald, *Appl. Phys. Lett.* **2004**, *85*, 22 5227.

[12] N. Khelifati, H. S. Laine, V. Vähänissi, H. Savin, F. Z. Bouamama, D. Bouhafs, *Phys Status Solidi A* **2019**, *216*, 17 1900253.

[13] S. Herlufsen, D. Macdonald, K. Bothe, J. Schmidt, *physica status solidi (RRL) – Rapid Research Letters* **2012**, *6*, 1 1.

[14] D. H. Macdonald, L. J. Geerligs, A. Azzizi, *J. Appl. Phys.* **2004**, *95*, 3 1021.

[15] L. Kimerling, J. Benton, *Physica B+C* **1983**, *116*, 1 297.

[16] X. Zhu, D. Yang, X. Yu, J. He, Y. Wu, J. Vanhellemont, D. Que, *AIP Adv.* **2013**, *3*, 8 082124.

[17] X. Zhu, X. Yu, P. Chen, Y. Liu, J. Vanhellemont, D. Yang, *Int. J. Photoenergy* **2015**, *2015* 154574.

[18] T. T. Le, Z. Zhou, A. Chen, Z. Yang, F. Rougieux, D. Macdonald, A. Liu, *J. Appl. Phys.* **2024**, *135*, 13 133107.

[19] K. Lauer, C. Möller, D. Debbih, M. Auge, D. Schulze, In *Gettering and Defect Engineering in Semiconductor Technology XVI*, volume 242 of *Solid State Phenomena*. Trans Tech Publications Ltd, **2016** 230–235.

[20] W. Wijaranakula, *J. Electrochem. Soc.* **1993**, *140*, 1 275.

[21] O. Olikh, V. Kostylyov, V. Vlasiuk, R. Korkishko, Y. Olikh, R. Chupryna, *J. Appl. Phys.* **2021**, *130*, 23 235703.

[22] J. D. Murphy, K. Bothe, M. Olmo, V. V. Voronkov, R. J. Falster, *J. Appl. Phys.* **2011**, *110*, 5 053713.

[23] O. Olikh, V. Kostylyov, V. Vlasiuk, R. Korkishko, R. Chupryna, *J. Mater. Sci.: Mater. Electron.* **2022**, *33*, 16 13133.

[24] D. Macdonald, T. Roth, P. N. K. Deenapanray, K. Bothe, P. Pohl, J. Schmidt, *J. Appl. Phys.* **2005**, *98*, 8 083509.

[25] M. Libra, V. Poulek, P. Kourim, *Research in Agricultural Engineering* **2017**, *63*, 1 10.

[26] S. Bowden, R. A. Sinton, *J. Appl. Phys.* **2007**, *102*, 12 124501.

[27] S. Schäfer, R. Brendel, *IEEE J. Photovolt.* **2018**, *8*, 4 1156.

[28] M. A. Green, *Prog. Photovoltaics Res. Appl.* **2022**, *30*, 2 164.

[29] S. C. Baker-Finch, K. R. McIntosh, D. Yan, K. C. Fong, T. C. Kho, *J. Appl. Phys.* **2014**, *116*, 6 063106.

[30] D. Klaassen, *Solid-State Electron.* **1992**, *35*, 7 953.

[31] T. Niewelt, B. Steinhauser, A. Richter, B. Veith-Wolf, A. Fell, B. Hammann, N. Grant, L. Black, J. Tan, A. Youssef, J. Murphy, J. Schmidt, M. Schubert, S. Glunz, *Sol. Energ. Mat. Sol.* **2022**, *235* 111467.

[32] L. E. Black, D. H. Macdonald, *Sol. Energ. Mat. Sol.* **2022**, *234* 111428.

[33] A. W. Mohamed, A. A. Hadi, K. M. Jambi, *Swarm Evol. Comput.* **2019**, *50* 100455.

[34] N. Klyui, V. Kostylyov, A. Rozhin, V. Gorbulik, V. Litovchenko, M. Voronkin, N. Zaika, *Opto-Electr. Rev.* **2000**, *8*, 4 402.